533385

Mesoscopic Nonlinear Elastic Modulus of Thermal Barrier Coatings Determined by Cylindrical Punch Indentation

J.I. Eldridge, D. Zhu, and R.A. Miller, NASA Glenn Research Center, Cleveland, OH 44135

Abstract

Cylindrical punch indentations are performed to determine the effective modulus of a plasma-sprayed ZrO_2-8wt%Y_2O_3 thermal barrier coating (TBC) as a function of coating depth. Cylindrical punch indentations offer significant advantages over pointed (Vickers, Berkovich, or Knoop) indentations for materials that do not exhibit linear elastic behavior. Cyclic loading with a cylindrical punch clearly shows the TBCs to exhibit nonlinear elastic behavior with significant hysteresis that is related to the compaction and internal sliding within the plasma-spray splat microstructure. In addition, the effect of a high heat flux laser treatment was shown to produce a gradient both in the effective TBC modulus and degree of loading/unloading hysteresis with depth.

I. Introduction

In order to survive service conditions, thermal barrier coatings (TBCs) must exhibit exceptional strain tolerance. Since a low elastic modulus is usually associated with high strain tolerance, a method of determining changes in elastic modulus would be a useful diagnostic tool and provide input for life prediction. Microindentation has been shown to be a useful technique for determining the elastic modulus of coatings.[1-4] Microindentation offers several advantages over conventional mechanical testing. Local variations in modulus may be examined and testing does not require separating the coating from the substrate. Non-instrumented Knoop indentation[5-7], instrumented spherical ball indentation[8-9], and Vickers indentation[10] have all been applied to determine the elastic modulus of TBCs.

An important complication in determining the elastic modulus of plasma-sprayed TBCs is that they do not exhibit linear elastic behavior.[11-14] For example, Choi et al.[13,14] showed that the effective modulus of a freestanding plasma-sprayed yttria-stabilized zirconia TBC specimen, as calculated from the slope of the stress-strain curve obtained from a compression test, varied from less than 35 GPa to almost 200 GPa over the course of an individual load/unload cycle. Therefore, modulus values must be associated with a stress level as well as stress history. Unfortunately, both non-instrumented Knoop and instrumented Vickers indentation do not allow a controlled variation of applied contact stress since the indent area increases with the applied load resulting in the applied contact stress being approximately equal to the coating hardness (load divided by contact area). In addition, data analysis for these tests assumes a constant elastic modulus. These limitations are removed by using a flat-bottomed cylindrical punch where the contact area remains constant during the entire load/unload cycle so that applied contact stress is linearly related to applied load. This communication describes the application of instrumented cylindrical punch indentation for measuring the local elastic modulus of plasma-sprayed yttria-stabilized zirconia TBCs as a function of applied contact stress. As an example,

this method is used to reveal changes in the elastic behavior as a function of depth that occur after subjecting the plasma-sprayed TBC to a severe high heat flux.

II. Experimental Procedure

The TBC specimens consisted of an approximately 1.5 mm thick plasma-sprayed ZrO_2-8wt%Y_2O_3 (YSZ) coating above a 0.25 mm thick Fe-25wt%Cr-5wt%Al-5wt%Y bond coat that was sprayed onto a 12.5 mm thick 4140 steel substrate. In addition to an as-sprayed specimen, a second specimen was exposed to an extreme high heat flux (about 250 W/cm^2) produced by a 5 sec exposure to a 1000 W CO_2 laser (beam waist diameter approximately 1.6 cm). This exposure was severe enough to produce a melted layer at the surface of the YSZ overcoat. Polished cross-sections of the YSZ-coated specimens were prepared for indentation testing. Both as-sprayed and heat-treated specimens were cross-sectioned, potted in epoxy, and polished to a 0.1 μm finish.

Indentations were carried out on the coating cross-sections using a desktop fiber push-out apparatus[15] with fixturing modified for indentation. The testing apparatus provides both load and displacement data, with the displacement data generated by a pair of symmetrically placed capacitance displacement gauges. The indenter was a 127 μm diameter flat-bottomed cylindrical tungsten carbide punch (National Jet Co., LaVale, MD) The specimen was clamped securely to the top of an x-y-z translation stage, which was used to generate sequences of indentations at 250 μm intervals across the cross-section of the YSZ overcoat. (Note that the absence of significant plastic deformation under the cylindrical punch allows the indentations to be positioned closer together without interaction than if a pointed indenter was used.) The motorized vertical translation stage pushes the specimen against the stationary punch; the stage was operated at a speed of 1 μm /sec, moving upward during loading and downward during unloading.

To avoid contributions from impression creep, the indent contact area was preconditioned by overloading before the actual test. This procedure successfully prevents coating creep during the test, which would produce a lower loading slope and higher unloading slope than would be obtained in the absence of creep.[1] Preloading to 20 N (4 cycles with 15 sec hold at maximum load) was performed before the actual test indentation to 15 N (3 cycles with 10 sec hold at maximum load). This procedure results in quite repeatable, closed-loop load/unload cycles, except for a small deviation for the first loading (Fig. 1). This simple preconditioning procedure is an added advantage of using a flat-bottomed cylindrical punch and cannot be applied with Vickers (or other increasing cross-section) indenters where preloading above the maximum test load will increase the indent contact area.

III. Analysis

Elastic modulus values were calculated using the relationship developed by Sneddon[16] for the elastic penetration of a flat-bottomed cylindrical punch with radius r into a half space:

$$P = \frac{4\mu r h}{1-\nu} \qquad (1)$$

where P is the applied load, h is the penetration distance of the indenter into the half space, μ is the shear modulus, and ν is Poisson's ratio of the material composing the half-space ($\nu_{TBC} = 0.25$ was selected for all TBC indentations). Pharr, Oliver, and Brotzen[2] showed that this equation could be rewritten in terms of Young's elastic modulus, E, and the slope of the loading/unloading curve, dP/dh:

$$\frac{dP}{dh} = \frac{2rE}{(1-\nu^2)} \tag{2}$$

Unlike the situation with a sharp indenter where Equation 2 holds only during initial unloading, the equation is valid for the entire loading/unloading cycle for a flat-bottomed cylindrical punch.

Before Equation 2 is applied, a compliance correction must be subtracted from the measured displacement, h_{raw}:

$$h = h_{raw} - C_{machine}P \tag{3}$$

where $C_{machine}$ is the machine compliance, which includes the entire punch compliance and that portion of the load train between where the capacitance gauges and targets are mounted. The effective machine compliance is determined from indentations on the 4140 steel substrate on the same polished cross-section, using Equation 1:

$$C_{total} = C_{machine} + C_{specimen} \tag{4}$$

$$C_{total}(P) = \frac{h_{raw}}{P} = C_{machine}(P) + \frac{(1-\nu_{substrate}{}^2)}{2rE_{substrate}} \tag{5}$$

where $E_{substrate} = 207$ GPa and $\nu_{substrate} = 0.3$ for 4140 steel. A look-up table of machine compliance vs. applied load is generated from the substrate indentation, and is used to make the compliance corrections for the coating indentations using Equation 3. The use of a machine compliance with a dependence on P is used because the P vs. h_{raw} curves for the substrate show a slight increase in slope, towards an asymptotic value, with increasing load. The machine compliance correction limits the successful application of this approach to specimens with a sufficiently low modulus (such as the porous plasma-sprayed TBC) so that the contact displacement is a significant fraction of the total measured displacement.

The slopes of the loading/unloading curves from the TBC indentations are determined from first fitting each loading or unloading segment to a power law relationship:[1]

$$P = k(h - h_f)^m \tag{6}$$

where k, h_f, and m are fitting constants, and separate fits are generated for each loading and unloading curve. Fitting is performed over the range of 5 N to P_{max}. Data below 5 N load were

not included in the fits to avoid the influence of the low-load region, where there is likely to be an indenter seating effect until full contact between the flat bottom of the punch and the specimen is attained. The loading/unloading slopes are then calculated by differentiating Equation 6:

$$\frac{dP}{dh} = mk(h - h_f)^{m-1} \qquad (7)$$

The modulus, E, can then be calculated using Equation 2 and plotted as a function of applied contact stress, $\sigma = P/\pi r^2$.

IV. Results and Discussion

Plots of a typical sequence of three loading/unloading cycles applied to the polished laser-treated TBC cross-section are presented in Fig. 1, both for indents in the melted surface layer as well as in the TBC interior. In contrast to the behavior observed for the melted zone, the TBC interior shows very nonlinear behavior with considerable hysteresis. This is also reflected in the relationship between the calculated modulus vs. applied contact stress determined (using Equations 2 and 7) from the final load/unload cycle for the same indentation from the TBC interior (Fig. 2). Modulus values were calculated from the loading/unloading slopes from 5 N (0.39 GPa) to 15 N (1.18 GPa). This plot shows that the modulus increases modestly during loading, experiences a discrete upward jump upon reversing loading direction, and then decreases more rapidly during unloading than it increases during loading. It should also be noted that the modulus determined during initial unloading, where it is determined by Vickers indentation, is higher than at any other point in the cycle.

A sequence of indentions at 250-μm intervals was performed across the cross-section of the as-sprayed YSZ coating. For each indentation, plots similar to Fig. 2 were generated. Fig. 3a summarizes the results by plotting the modulus determined at the end of the final loading cycle (at P_{max}=15 N) and at the beginning of the final unloading cycle (again at P_{max}=15 N). These modulus values correspond to the endpoints (maximum contact stress) of the modulus vs. contact stress curves, which Fig. 2 shows is where the difference between the loading and unloading modulus is the greatest. The difference between these modulus values represents a discontinuity at the loading/unloading transition and is associated with hysteresis during load cycling. For the as-sprayed coating, both modulus values (as well as their difference) remain constant across the YSZ thickness.

A sequence of indentations at 250-μm intervals was also performed across the cross-section of the laser-treated YSZ coating. Fig. 3b plots the modulus determined for each indent at the end of the final loading cycle as well as at the beginning of the final unloading cycle. In this case, a modulus gradient is evident, with the modulus decreasing from the outer surface (where a melted layer is present). In addition, the discontinuity between the loading and unloading modulus values (vertical distance between circles and squared in Fig. 3) decreases towards the surface and essentially vanishes in the melted layer where hysteresis is not observed. Note that the diameter

of the indent is relatively large (127 μm), about half the thickness of the melted layer, so that the near-surface indentation may be influenced by the surrounding epoxy (low modulus) as well as the underlying unmelted YSZ.

Figs. 1 and 2 clearly demonstrate the nonlinear hysteretic behavior of plasma-sprayed TBCs under cyclic compression. Despite the nonlinear behavior, the cycles are closed-loop and return to the original displacement; this complete recovery is an indication of elastic behavior. The observed stiffening under applied load and hysteresis can be modeled by a combination of compaction (which produces stiffening) and internal sliding (which causes hysteresis) of the splats within the plasma-spray microstructure.[12] Loading/unloading hysteresis is observed because static friction must be overcome before reverse internal sliding can occur during unloading. More generally, this type of behavior is observed in a broad range of consolidated materials and has been labeled nonlinear mesoscopic elasticity[17] because the elastic behavior is largely governed by the contacts between the material subelements (in this case the individual splats).

As shown in Fig. 3, the high heat flux laser treatment resulted in significant changes in the TBC elastic behavior as a function of depth. The laser-treated TBC shows a clear decrease in both the unloading and loading modulus values across the coating thickness. In addition, the difference between the unloading and loading modulus at maximum load (vertical distance between circle and square symbols in Fig. 3), decreases towards the surface of the laser-treated TBC. This corresponds to a decrease in hysteresis and therefore a decrease in internal sliding; in fact, the hysteresis disappears completely in the surface melted layer, which no longer exhibits the plasma-spray splat microstructure. The measurement of loading/unloading hysteresis therefore may be a useful tool for ascertaining the degree of internal sliding associated with a plasma-spray splat microstructure.

V. Conclusions

Because plasma-sprayed TBCs show nonlinear mesoscopic elastic behavior, the use of a cylindrical punch offers significant advantages over the use of pointed indenters for determining the effective modulus of the coating as a function of applied contact stress. The advantage of the cylindrical punch is twofold: (1) below a limiting applied contact stress, deformation is purely elastic over the complete load/unload cycle, and (2) the constant contact area results in the applied contact stress being proportional to the applied load. Therefore, the effective modulus can be determined over the complete load/unload cycle (compared to just during initial unloading for pointed indenters), and the load/unload cycle spans a well-controlled range of applied contact stress (applied contact stress is not well controlled with pointed indenters because contact area increases with increased applied load).

Cylindrical punch indentation was successfully applied to determine gradients in TBC modulus with depth produced by exposure to a high heat flux. In addition, the measured loading/unloading hysteresis was shown to be a useful diagnostic criterion for internal sliding, which is an important mechanism for providing TBC strain tolerance.

References

1. W.C. Oliver and G.M. Pharr, "An Improved Technique for Determining Hardness and Elastic Modulus Using Load and Displacement Sensing Indentation Experiments," J. Mater. Res., 7[6], 1564-83 (1992).
2. G.M. Pharr, W.C. Oliver, and F.R. Brotzen, "On the Generality of the Relationship Among Contact Stiffness, Contact Area, and Elastic Modulus during Indentation," J. Mater. Res., 7[3], 613-17 (1992).
3. M.F. Doerner and W.D. Nix, "A Method for Interpreting the Data from Depth-Sensing Indentation Instruments," J. Mater. Sci., 1[4], 601-9 (1986).
4. D.B. Marshall, T. Noma, and A.G. Evans, "A Simple Method for Determining Elastic-Modulus-to-Hardness Ratios Using Knoop Indentation Measurements," J. Amer. Ceram. Soc., 65[10], C-175 to C-176 (1982).
5. S.-H. Leigh, C.K. Lin, and C.C. Berndt, "Elastic Response of Thermal Spray Deposits under Indentation Tests," J. Amer. Ceram. Soc., 80[8], 2093-99 (1997).
6. J.P. Singh, M. Sutaria, and M. Ferber, "Use of Indentation Technique to Measure Elastic Modulus of Plasma-Sprayed Zirconia Thermal Barrier Coating," Ceram. Eng. Sci. Proc., 18[4], 191-200 (1997).
7. D. Zhu and R.A. Miller, "Thermal Conductivity and Elastic Modulus Evolution of Thermal Barrier Coatings under High Heat Flux Conditions," J. Thermal Spray Technol., 19, 175-180 (2000).
8. J.S. Wallace and J. Ilavsky, "Elastic Modulus Measurements in Plasma Sprayed Deposits," J. Thermal Spray Technol., 7[4], 521-6 (1998).
9. A. Pajares, L. Wei, B.R. Lawn, N.P. Padture, and C.C. Berndt, "Mechanical Characterization of Plasma Sprayed Ceramic Coatings on Metal Substrates by Contact Testing," Mater. Sci. Eng. A, 208, 158-65 (1996).
10. D. Basu, C. Funke, and R.W. Steinbrech, "Effect of Heat Treatment on Elastic Properties of Separated Thermal Barrier Coatings," J. Mater. Res., 14[12], 4643-50 (1999).
11. J.T. DeMasi-Marcin, K.D. Sheffler, and S. Bose, "Mechanisms of Degradation and Failure in a Plasma-Deposited Thermal Barrier Coating," ASME J. Eng. Gas Turbines Power, 112, 521-526 (1990).
12. E.F. Redja, D.F. Socie, T. Itoh, "Deformation Behavior of Plasma-Sprayed Thick Thermal Barrier Coatings," Surf. Coatings Technol., 113, 218-226 (1999).
13. S.R. Choi, D. Zhu, and R.A. Miller, "High-Temperature Slow Crack Growth, Fracture Toughness and Room-Temperature Deformation Behavior of Plamsa-Sprayed ZrO_2-8wt% Y_2O_3," Ceram. Eng. Sci. Proc., 19[4], 293-301 (1998).
14. S.R. Choi, D. Zhu, and R.A. Miller, "Deformation and Strength Behavior of Plasma-Sprayed ZrO_2-8wt%Y_2O_3 Thermal Barrier Coatings in Biaxial Flexure and Trans-Thickness Tension," Ceram. Eng. Sci. Proc., 21(4), 653-661 (2000).
15. J.I. Eldridge, "Desktop Fiber Push-Out Apparatus," NASA Tech. Memo No. 105341, National Aeronautics and Space Administration, Cleveland, OH, 1991.
16. I.N. Sneddon, "The Relation between Load and Penetration in the Axisymmetric Boussinesq Problem for a Punch of Arbitrary Profile," Int. J. Engng. Sci., 3, 47-57 (1965).

17. R.A. Guyer and P.A. Johnson, "Nonlinear Mesoscopic Elasticity: Evidence for a New Class of Materials," Physics Today, 52(4), 30-36 (1999).

Figure Captions

Fig. 1. Typical sets of three consecutive cylindrical punch loading/unloading cycles performed on polished cross-section of laser-treated TBC. (left) melted surface layer. (right) TBC interior. Note small deviation between first and subsequent loadings for TBC interior.

Fig. 2. Calculated modulus vs. applied contact stress determined from final (third) indentation cycle in the TBC interior from Fig. 1.

Fig. 3. Modulus calculated at P_{max} (15 N) at the end of the final loading cycle (open square) and at the beginning of the final unloading cycle (open square) as a function of distance from the TBC surface. (a) as-sprayed TBC. (b) laser-treated TBC.

Fig. 1

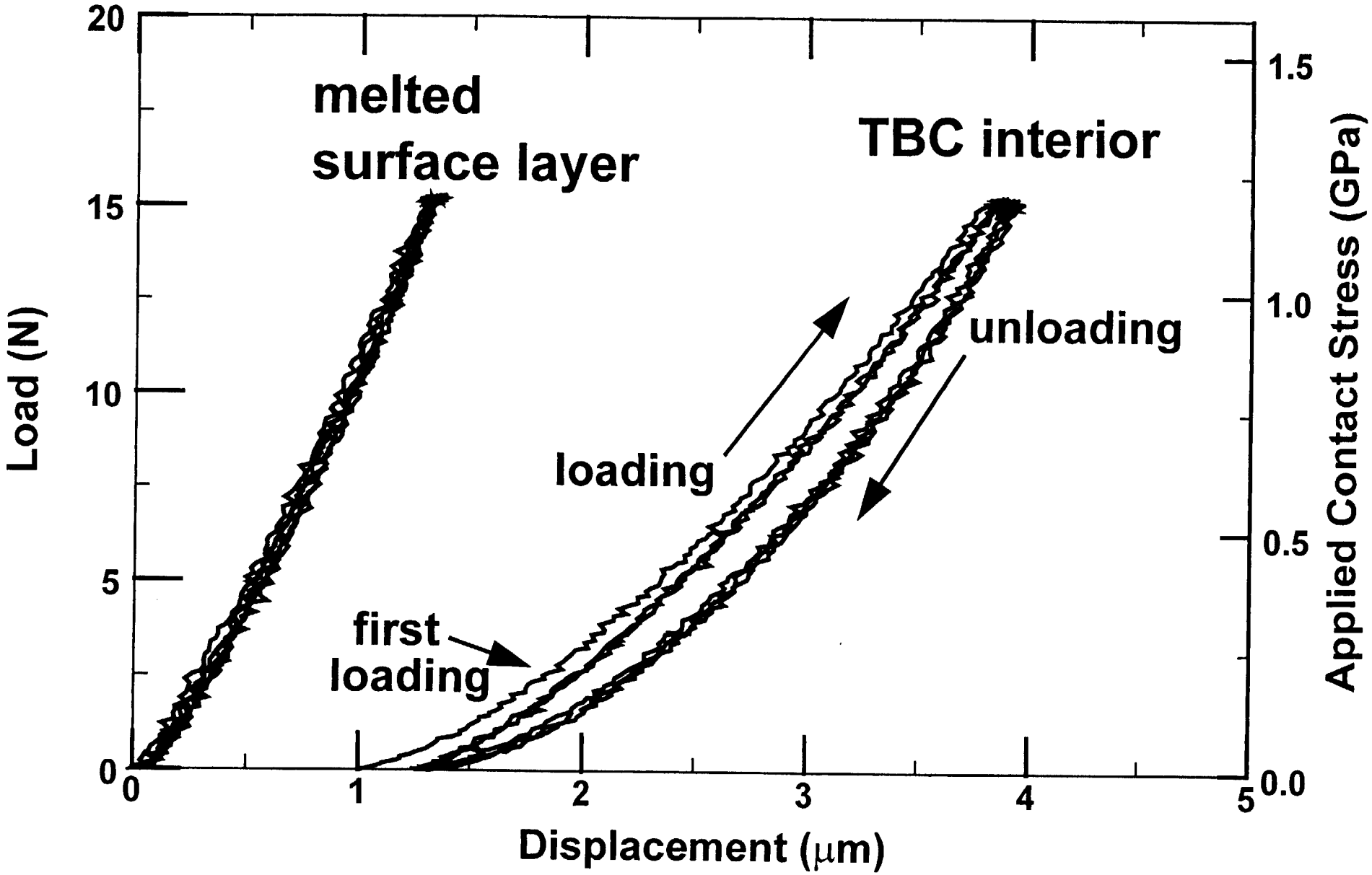
melted
surface layer
TBC interior
loading
unloading
first
loading
Load (N)
Applied Contact Stress (GPa)
Displacement (μm)
0
5
10
15
20
0.0
0.5
1.0
1.5
0
1
2
3
4
5

Fig. 2

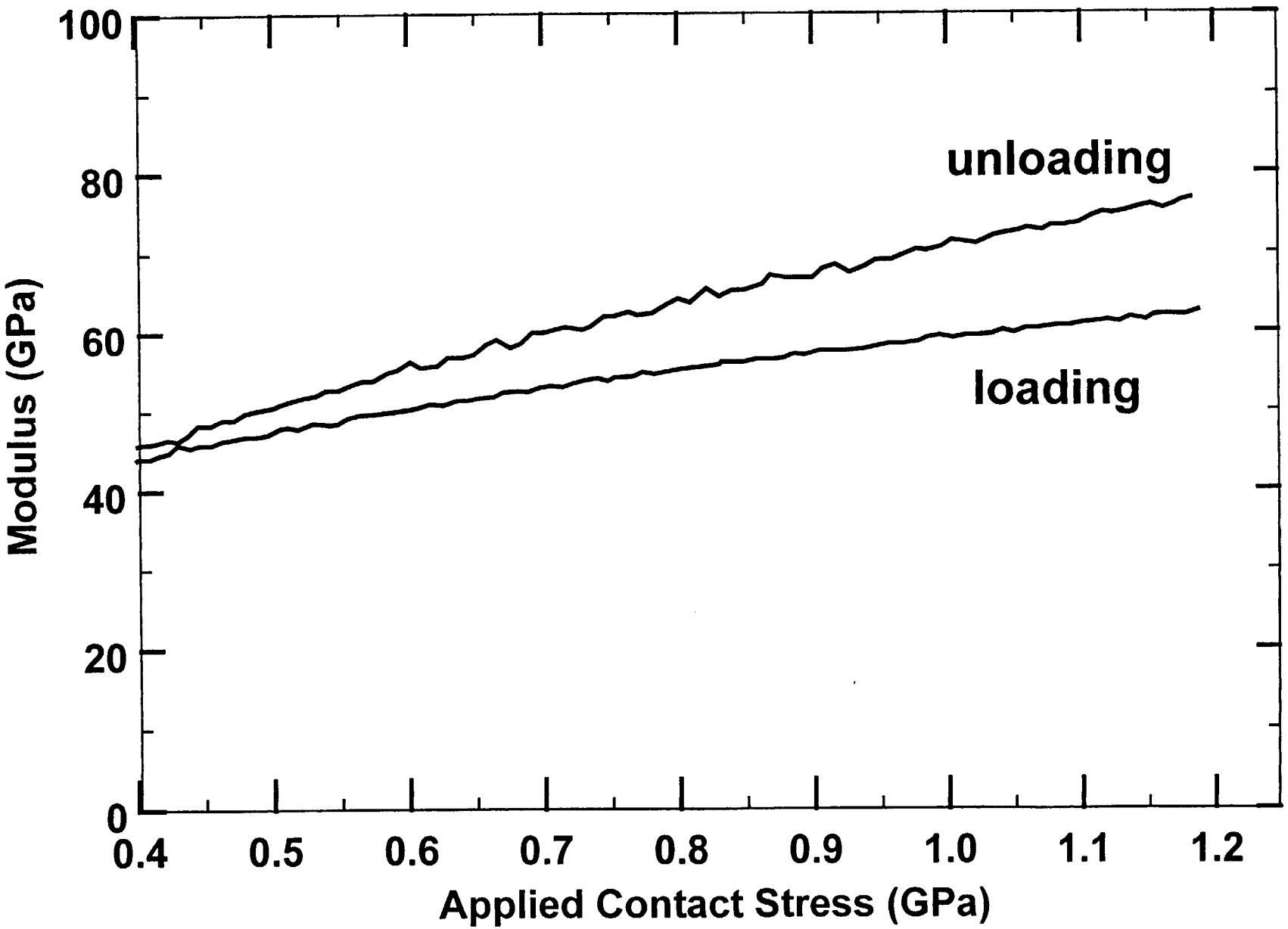
100
80
60
40
20
0
Modulus (GPa)
unloading
loading
0.4
0.5
0.6
0.7
0.8
0.9
1.0
1.1
1.2
Applied Contact Stress (GPa)

Fig. 3a

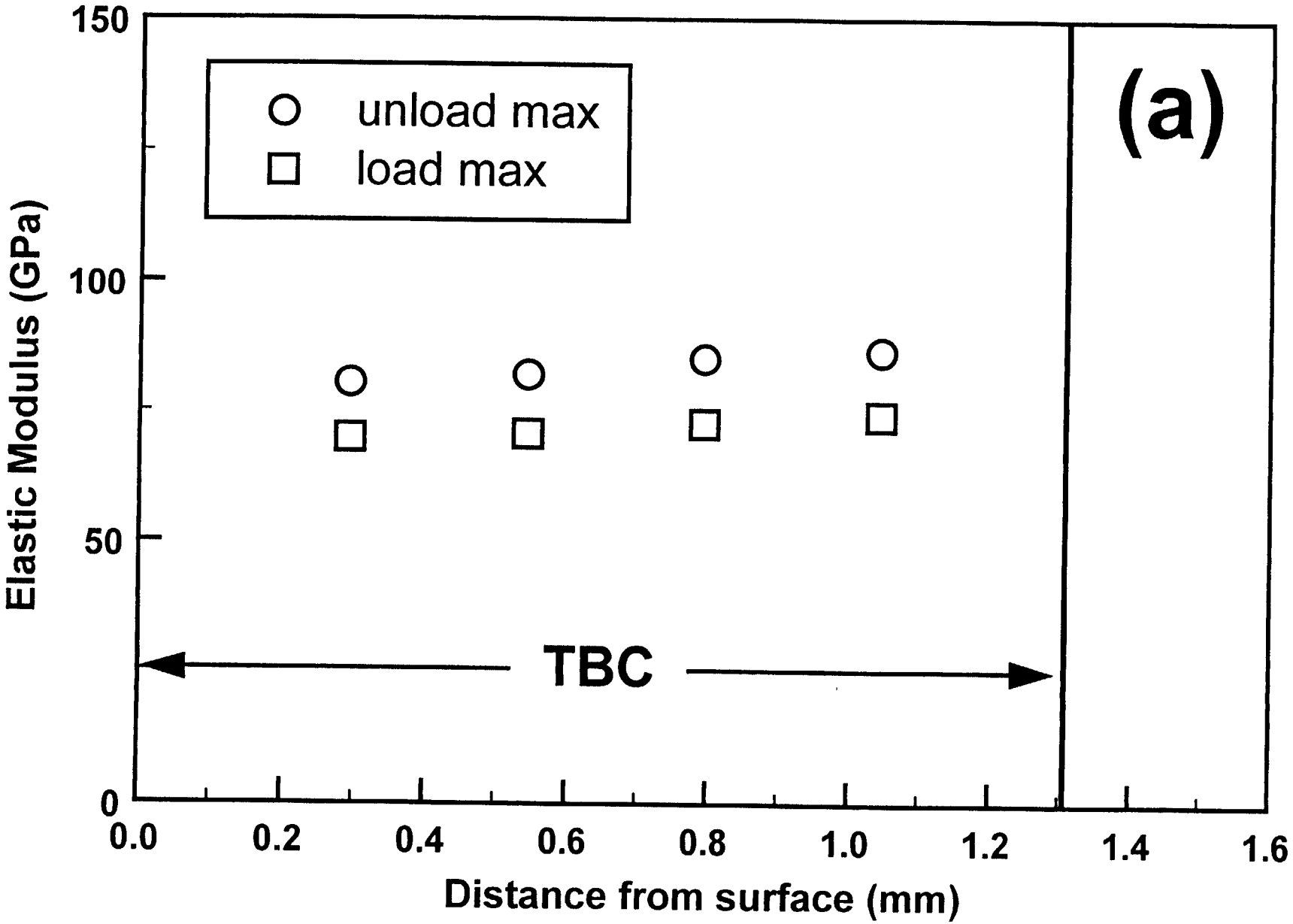
150
100
50
0
Elastic Modulus (GPa)
unload max
load max
(a)
TBC
0.0
0.2
0.4
0.6
0.8
1.0
1.2
1.4
1.6
Distance from surface (mm)

Fig. 3b

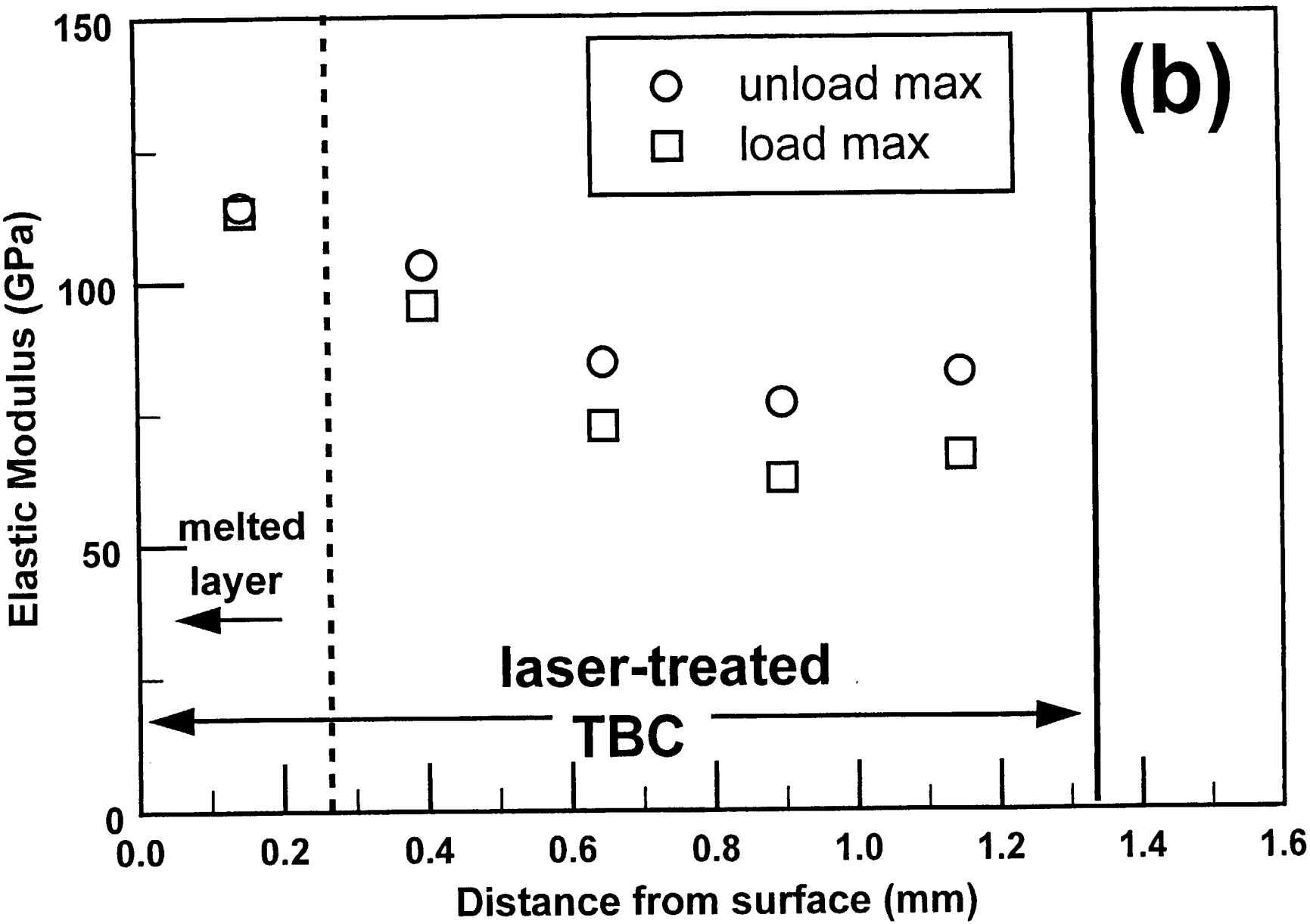
(b)
unload max
load max
Elastic Modulus (GPa)
150
100
50
0
melted
layer
laser-treated
TBC
0.0
0.2
0.4
0.6
0.8
1.0
1.2
1.4
1.6
Distance from surface (mm)